Characterization of an aluminum conductor steel reinforced (ACSR) after 60 years of operation

F. Lequien, Q. Auzoux, G. Moine, M. Rousseau, S. Pasquier-Tilliette, A. Holande, S. Ammi, S. Heurtault, P. Prieur

Version of Record: https://www.sciencedirect.com/science/article/pii/S1350630720315636
Manuscript_c5f7ff504fe0413272cdf3527d89c072

Characterization of an aluminum conductor steel reinforced (ACSR) after 60 years of operation

F. LEQUIEN[1*], Q. AUZOUX[1], G. MOINE[1], M. ROUSSEAU[1], S. PASQUIER-TILLIETTE[1], A. HOLANDE[1], S. AMMI[2], S. HEURTAULT[2] and P. PRIEUR[2]

[1] Den-Service de la Corrosion et du Comportement des Matériaux dans leur Environnement (SCCME), CEA, Université Paris-Saclay, F-91191, Gif-sur-Yvette, France

[2] Réseau de Transport et d'Électricité, CNER – Département Liaisons, Immeuble Window – 7C Place du Dôme - 92073 Paris la Défense cedex

*Corresponding author

E-mail address of the authors : florence.lequien@cea.fr, quentin.auzoux@cea.fr, gervaise.moine@cea.fr, matthias.rousseau@cea.fr, sidonie.pasquier-tilliette@cea.fr, aurore.holande@cea.fr, soraya.ammi@rte-france.com, stephane.heurtault@rte-france.com, pascale.prieur@rte-france.com.

Abstract

An aluminum conductor steel reinforced (ACSR) extracted from an overhead power line operated in Northern France during more than 60 years was characterized together with a more recent equivalent conductor. Visual inspection, local observation and chemical analysis by Scanning Electron Microscope (SEM) and Energy Dispersive Spectroscopy (EDS) as well as Raman spectroscopy were used to characterize the microstructure of the strands and to evidence signs of corrosion or potential degradation. Analysis of the grease was done by Fourier Transform InfraRed Spectroscopy (FTIR). The mechanical properties of the strands were evaluated by constant strain rate tensile test at ambient temperature. Hardness was measured as well. Partial oxidation of the steel galvanization layer, degradation of the grease – especially oxidation due to ageing – and atmospheric corrosion pits on the external layer of aluminum strands were evidenced. The mechanical properties of the galvanized steel strands were still in agreement with the requirements of the standards edited in 1955 contrarily to the mechanical properties of the external layer aluminum strands, indicating a potential deleterious effect of the corrosion pits. The tensile strength of the conductor estimated from the mechanical properties of its constitutive strands was slightly higher than the requirements of the standards edited in 1955 and slightly lower than the more demanding requirements of recent standards.

Keywords

Aluminum, steel, conductor, power line, durability

Highlights

- A conductor from a power line operated during more than 60 years was characterized
- Corrosion of the strands and ageing of the grease were evidenced
- The mechanical properties of the steel strands still fulfilled the 1955 standards

1 Introduction

In France, the major part of the electricity produced is transmitted by overhead power lines, which are composed of towers, conductors, guard cables and insulators. The conductors consist of helically wound aluminum alloys and galvanized steel strands. There are different types of conductors, such as aluminum conductor steel reinforced (ACSR) and all aluminum alloys conductor (AAAC). France currently has over 100,000 km of overhead power lines, some of which are in service for over 50 years. A first assessment conducted on the damage rate showed that it is more important after 60 years of operation with an increased risk of strand rupture [1-3]. In order to optimize the maintenance of the existing lines, an identification of the critical degradation processes is necessary. Some of them are relatively well known, namely wear [4-6], fatigue [7-12], corrosion [1, 13-20] and fretting corrosion[21].

Apart from the zones where the mechanical loading is exacerbated due to the connection devices, the principal damage mechanism of ACSR conductors is the corrosion of the aluminum strands. Two types of corrosion were identified: i) atmospheric corrosion of the strands exposed to the environment which induces a uniform attack often accompanied by deep pitting [13, 15, 16] ; ii) galvanic corrosion due to the presence of dissimilar metals (aluminum, zinc and steel) together with an electrolyte. Under the later circumstances, the aluminum strands may act as the anode of the galvanic cell and thus be corroded relatively rapidly which may lead to the premature failure of the conductor [13, 14, 16, 17]. The corrosion kinetics is also known to be faster in marine or highly industrial environment than in average rural or urban environment [4, 15, 22-26]. In order to prevent this type of corrosion, penetration of corrosive aqueous solutions may be avoided – or at least delayed – by the use of grease [13, 16, 18].

The estimation of the actual properties and residual life of individual conductors is complex because it depends on numerous parameters, such as the conductor design and its constitutive materials, the environmental conditions and the mechanical loading. Therefore, a control policy are used by mostly all Transmission System Operators, based on infrared detection of hot spots or electromagnetic estimation of the remaining zinc thickness or remaining steel cross section [1, 14]. In order to optimize these non-destructive controls, more information on the relation between actual properties and inspection results is needed.

In this framework, the aim of the present work was to characterize an ASCR conductor extracted from a 225 kV overhead transmission line, which had been operated since 1950. Visual inspection, local observation and chemical analysis by Scanning Electron Microscope (SEM) and Energy Dispersive Spectroscopy (EDS) as well as Raman spectroscopy were used to characterize the microstructure of the strands and the signs of corrosion or potential degradation. Analysis of grease was done by Fourier Transform InfraRed Spectroscopy (FTIR). The mechanical properties of the

strands were evaluated by constant rate tensile test at ambient temperature. Hardness was measured as well. The conformity of the strands to the standards was evaluated, and related to the ageing causes.

2 Materials and experimental procedures

2.1 Materials

The samples of the studied ACSR conductor were extracted from the Guarbecque-Holque-Woesthyne (GHW) overhead power line, in service since 1950 in northern France. The samples were cut in 2011, after more than 60 years of operation. As presented in Figure 1, this conductor was composed of aluminum and galvanized steel strands: 19 galvanized steel strands with a nominal diameter of 2.4 mm divided into three layers (1 + 6 + 12) in the center part and 32 aluminum strands with a nominal diameter of 3.6 mm distributed in two external layers (13 + 19). The conductor had a nominal outer diameter of 26.4 mm. The overall nominal section was 412 mm^2. Figure 1 also shows a cross section of a more recent equivalent conductor that was not in operation but was also characterized. This latter conductor, labelled as “modern” in the rest of the study, was used as a reference to highlight potential degradations of the GHW conductor. The two conductors were completely greased, except for the outer layer, which was exposed to the environment.

The GHW overhead power line is located in a mixed urban-rural environment. Data from the nearest meteorological station located in Dunkerque are reported in Table 1. The average temperature is 11.6 °C with a relative humidity slightly higher than 80%. The wind speed is up to 7.5 m/s. The coast is not in the vicinity which explains the low chloride concentration (3 mg/m²d). The average sulfur dioxide concentration in France is also low (< 5 $\mu g.m^{-3}$) [27].

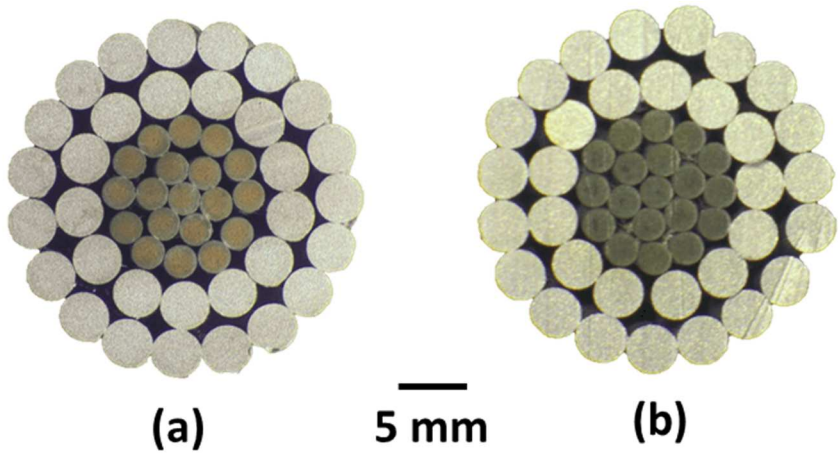

Figure 1: Cross sections of the studied conductors (a) GHW and (b) modern. The two outer layers were made of aluminum. The internal strands were made of galvanized steel.

Table 1 : Environmental parameters of the GHW overhead power line. Temperature, relative humidity and wind speed are average values estimated over the period 1990-2015.

Average temperature (°C)	Relative humidity (%)	Wind speed (m/s)	Chloride concentration S_d (mg/m²d)	Sulfur dioxide concentration P_d (mg/m²d)

11.6	82	6.5-7.5	3	4

2.2 Chemical composition, microstructure and hardness

The carbon and sulfur content of the steel were measured by a LECO CS 244 analyzer. The accuracy for a 1 g sample was 2 ppm for sulfur and 5 ppm for carbon.

In order to characterize the microstructure and the hardness of the strands of the studied conductors, 2.5 cm long sections were cut with a wire saw. Three sections were cut from the GHW conductor and presented similar results. Only one section was cut from the modern conductor. The sections were first degreased and then embedded for preparation of the cross-sections. Degreasing was done by successive immersion of the sections in acetone and in the ultrasonic bath. The sections were then embedded in a conductive resin without separating the strands in order to localize each strand and to be able to observe potential interaction with the neighboring strands. Then the samples were ground with SiC paper and polished with diamond paste.

Macroscopic and microscopic observations were carried out using a scanning electron microscope (SEM) equipped with an electron dispersive spectrometry X-ray microanalysis system (EDS) for the elemental analysis of selected areas. SEM was also used to observe the fracture surfaces of the tested tensile samples.

The Raman measurements were carried out with a Renishaw Invia spectrometer. The wavelength was 532 nm and the power on the sample was around 100 µW. The magnification of the objective was × 50.

The Vickers micro hardness were carried out with a DuraScan 70 of Struers. Vickers micro hardness was measured on the polished cross sections using a ten g mass for the aluminum strands and a one kg mass for the steel strands. Five indents were done on each studied strand.

In order to collect information on the composition and the potential degradation of the grease, the degreasing baths were analyzed by FTIR after evaporation of the acetone. The amounts of metallic elements were estimated by inductively coupled plasma mass spectrometry (ICP-MS) after dissolution of the deposits. As only 10% to 20 % of the deposits was dissolved, the measured amounts might not reflect their exact concentration in the grease. Measurements of sulfur and chlorine contents could not be made because the recovered deposit was not soluble in toluene or xylene.

2.3 Tensile tests

For the tensile tests on individual strands, 350 mm long samples were cut from the conductors. In order to dissolve the grease and facilitate the separation of the strands without altering them, the samples were immersed in de-aromatized petroleum during one day. A ten minute sequence in an ultrasonic bath was imposed at the beginning and at the end of this immersion. Each strand was then cleaned with de-aromatized petroleum to remove the last residual traces of grease before a final stage of degreasing with ethanol. After observation of their surface, the strands were manually straightened. Six strands (three aluminum strands and three galvanized steel strands) were tested for each studied conductor.

The tensile tests were done at ambient temperature on an INSTRON electromechanical machine type 5969 and a 50 kN load cell. INSTRON self-clamping jaws were used. The test conditions were chosen on the basis of the following standards: NF EN ISO 6892-1 [28] and NF EN 50182 [29]. These tests were constant elongation rate tensile tests until fracture. The total length of the strands was 350 mm. The initial distance between the jaws was 250 mm (± 0.4%). The crosshead displacement was 0.5 $mm.s^{-1}$ (30 mm/min), which corresponded to a strain rate of 2 10^{-3} s^{-1}. The accuracy of the measure of the initial section area of the strands was ± 0.5%. The accuracy of the load cell was ± 0.25%. The elongation of the specimen was calculated from the crosshead displacement after subtraction of the elastic elongation of the loading line based on the following Young's modulus values: 210 GPa for steel and 70 GPa for aluminum.

3 Results

3.1 Galvanized steel strands

3.1.1 Chemical composition, microstructure and hardness

The steel of the two conductors contained 0.8 wt% of carbon, which is near the eutectoid composition. For the GHW conductor, the sulfur content was around 510 ppm, which was higher than the sulfur content of the modern conductor (around 50 ppm).

The Vickers hardness of the GHW galvanized steel strands was lower than the one of the modern conductor, between 420 and 470 HV and between 490 and 520 HV, respectively.

The steel strands were galvanized. The thickness of the galvanization layer of the steel strands of the modern conductor was between 25 and 70 µm. EDS analysis confirmed that the galvanization layer was made of iron and zinc (Figure 2). It consisted of two phases: a zinc-iron inner sublayer containing less than 6 wt% of iron, which is the zeta phase, and a pure zinc outer sublayer, which is the eta phase [30]. The thickness of the sublayers was different from one strand to another and from one position to another. The outer sublayer was thicker than the inner one, which was between 7 and 20 µm thick. The outer sublayer was oxidized up to a few micrometers depth, around 3 µm. The thickness of this ZnO layer never exceeded 5 µm. The amount of carbon detected during this EDS analysis was most certainly related to a contamination by the grease, which – despite degreasing – remained present as a thin film on the samples.

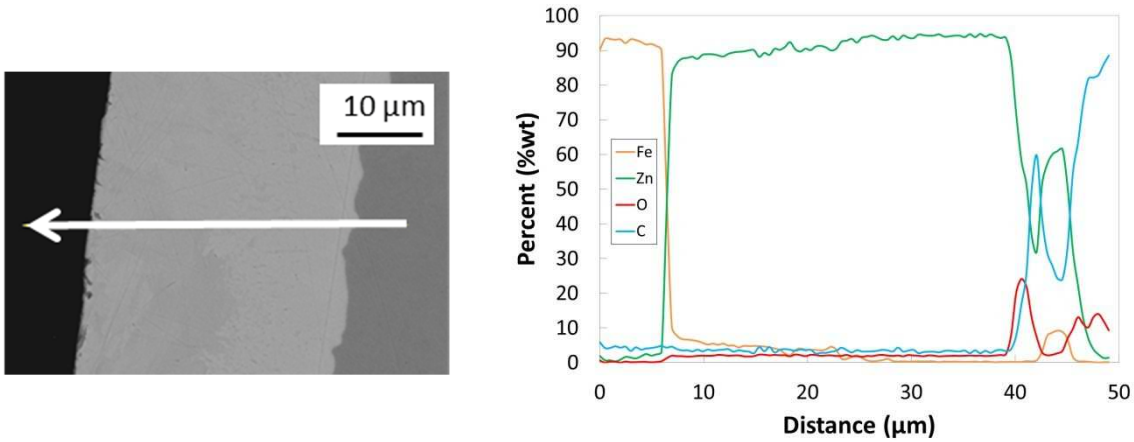

Figure 2: SEM image and EDS analysis of a cross section of the galvanization layer of the modern conductor. Fe is in orange, Zn in green, O in red and C is in cyan.

The galvanization layer of the GHW conductor presented different features depending on the studied strand and location. In most cases, the average thickness of the galvanization layer was lower than 20 µm and no pure zinc outer sublayer was observed (Figure 3(a)). The innermost sublayer was the delta phase, with a maximum iron content of 10 wt%. Its thickness was low: between 2 and 5 µm. The iron content of the second sublayer was between 4 and 6 wt%, which corresponded to the zeta phase.

On some strands of the outer layer of the steel part of the conductor, the galvanization layer was locally thicker (up to 30 µm) than in the general case described previously and presented a supplementary outer sublayer which appeared darker on SEM observations (Figure 3 (b)). EDS analysis showed that this sublayer contained mainly zinc and oxygen. However, the amount of carbon detected by EDS, which was most probably linked to the presence of grease, complicated the identification of this oxide. It was consequently characterized by Raman spectroscopy, which showed that this layer was amorphous or slightly crystallized ZnO with the three following characteristic peaks [31]: 165 cm^{-1} , 435 cm^{-1} and 565 cm^{-1} (Figure 4). Figure 3 (b) also indicated the partial oxidation of the zeta phase.

In some areas, the steel strands of the outer layer of the steel part of the conductor were locally embedded in their neighboring aluminum strand. In these areas, the galvanization layer was even thicker (up to 40 µm) and EDS analysis indicated the presence of unoxidized eta phase (Figure 3(c)).

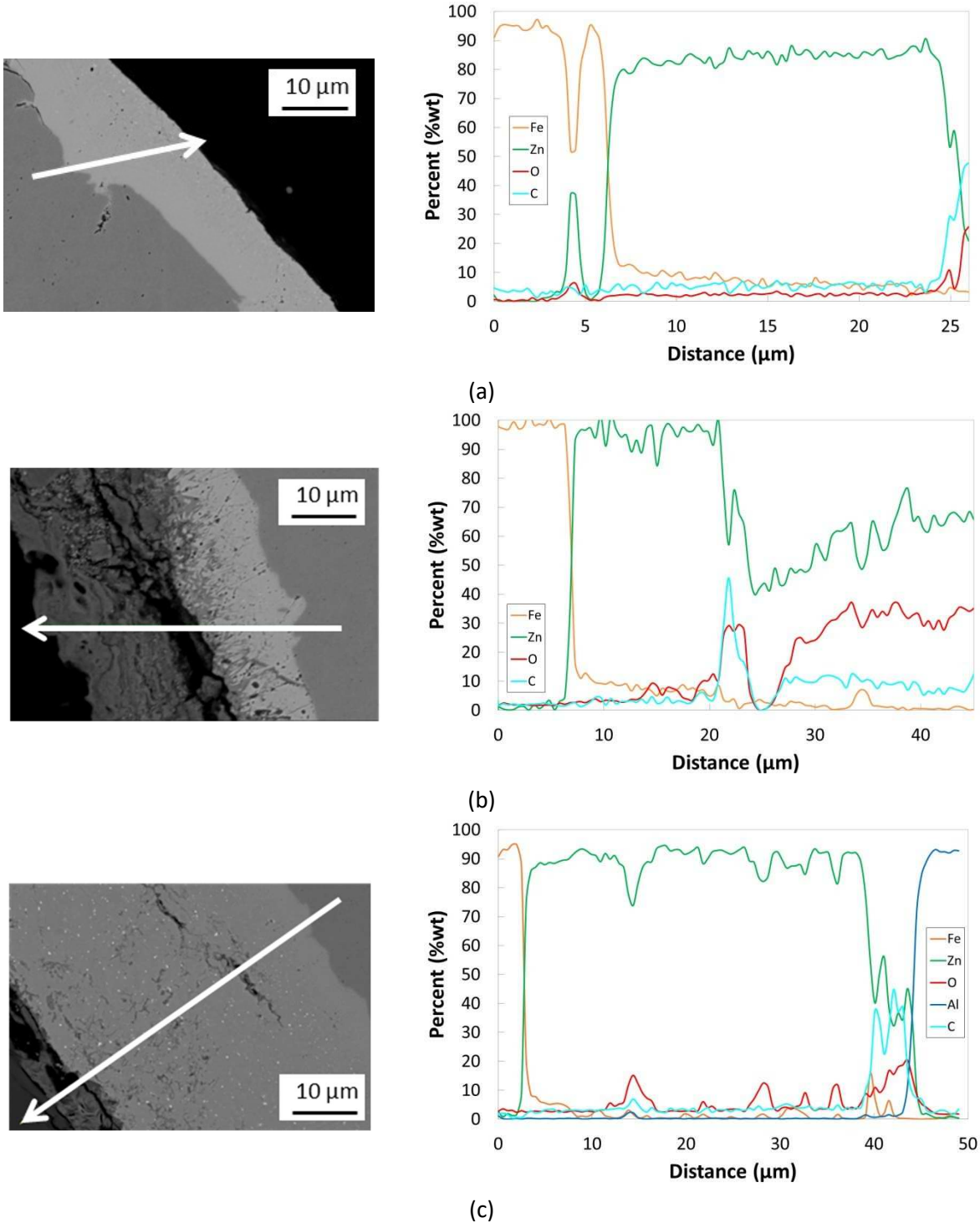

Figure 3: SEM images and EDS analysis of cross sections of the galvanization layer of the GHW conductor. (a) General case, (b) partially oxidized layer and (c) in the areas that are embedded in an aluminum strand. Iron is represented in orange, zinc in green, oxygen in red, carbon is in cyan and aluminum is in blue.

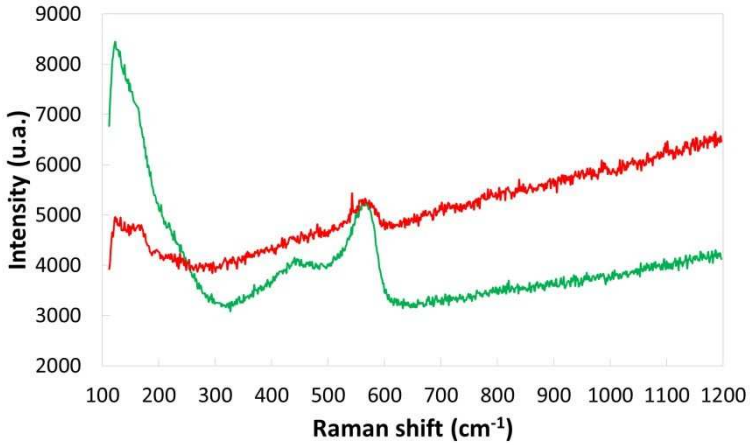

Figure 4: Raman spectra obtained on the galvanization layer of a strand from the outer layer of the steel part of the GHW conductor, in the partially oxidized inner sublayer (in red) and in the oxidized outer sublayer (in green).

Cracks were noticed on the cross section of some of the studied strands. Few and short (< 15 µm) for the modern conductor, their apparent length varied from 10 to 800 µm for the GHW conductor (Figure 5). SEM analysis revealed the presence of zinc along the length of the crack, indicating that cracks were present prior to the galvanizing. They were therefore considered as wire drawing defects. For the GHW conductor, inside the cracks, the galvanization layer was micro-cracked. Some of these micro-cracks appeared to connect the crack tip to the surface. However, the cross section sample showed that the steel did not appear corroded. In addition to oxygen, significant amount of chlorine were found along these cracks, and were more important in areas where the grease rose by capillarity at the studied surface.

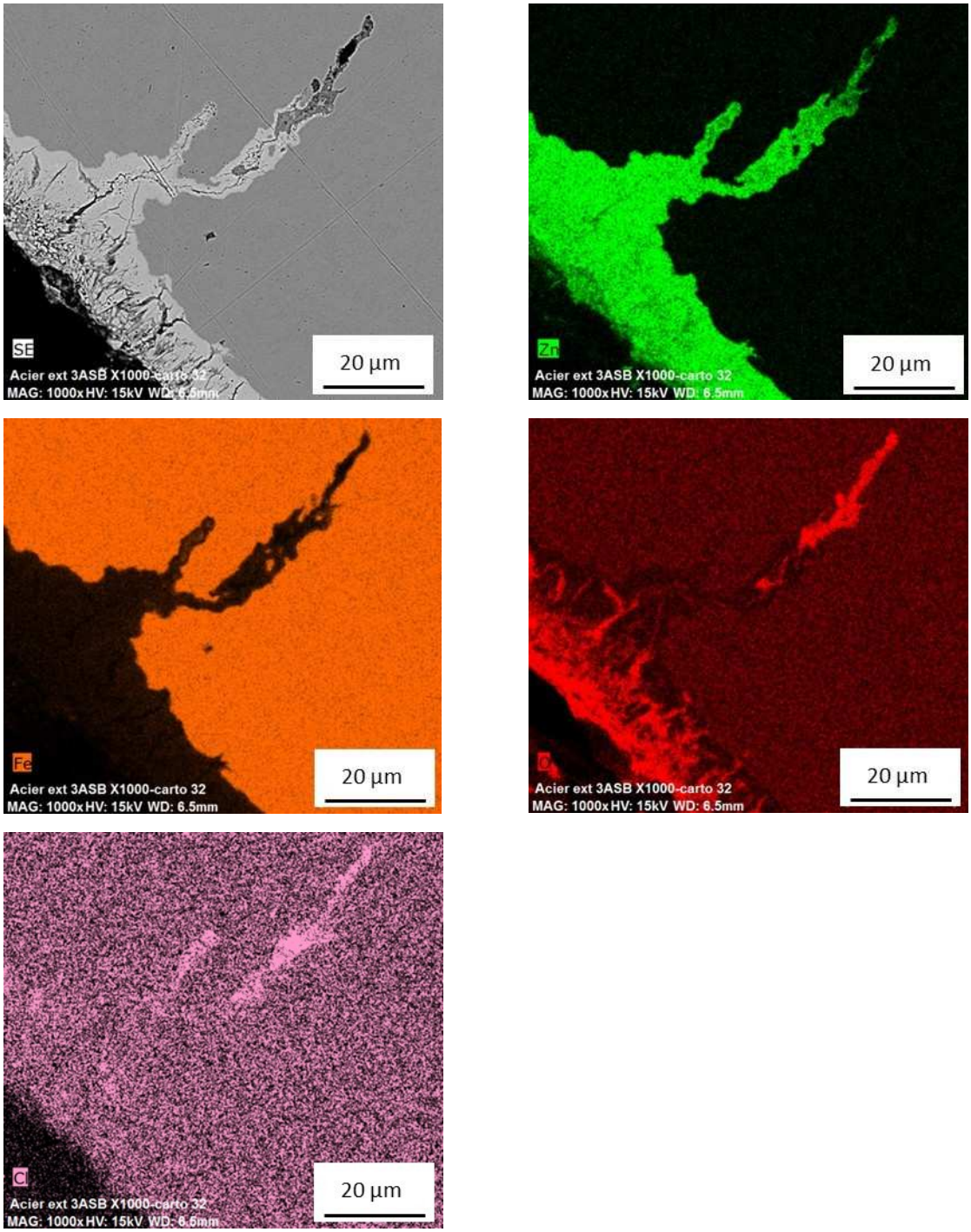

Figure 5: SEM images in secondary electrons mode and EDS analysis of a cross section of a crack near the surface of a galvanized steel strand of the GHW conductor, zinc in green, iron in orange, oxygen in red and chlorine in pink.

3.1.2 Tensile tests, pre- and post-test characterization

Before the tensile tests, the diameter of the galvanized steel strands was measured: 2.39 ± 0.01 mm and 2.40 ± 0.02 mm, for those extracted from the GHW and the modern conductor, respectively. Visual examination of the strands evidenced some corrosion marks. They were much more pronounced on the GHW conductor (Figure 6) than on the modern one (Figure 7). They were also more numerous on the external strands than on the central strands. On every strand extracted from either the GHW conductor or the modern one, periodic marks due to the interaction with neighboring strands were also noticed (left picture in Figure 7).

Tensile test results are plotted in Figure 8 and the corresponding mechanical properties are reported in Table 2. The GHW galvanized strands clearly had a lower strength and a higher elongation at fracture than the modern ones. This result is discussed in section 4.2. No clear difference between the mechanical properties of the three GHW tested strands was noticed apart from the reduction area at fracture, which was lower for the central strand (0.28) than for the two other tested strands (0.44).

After the tensile tests, fractured strands were observed by optical means and by SEM. Figure 9 indicates that the fracture of the galvanized steel strands extracted from the GHW conductor did not initiate on the corrosion marks. All the tested galvanized steel strands – extracted either from the GHW conductor or the modern one – fractured following a typical "cup-cone" ductile fracture mechanism. The central area of the fracture surface was globally oriented perpendicular to the tensile direction and consisted of numerous dimples (Figure 10). This area was surrounded by a ring-shaped slanted area, which consisted of sheared dimples. As the other tested strands, the central galvanized steel strand extracted from the GHW conductor presented a "cup-cone" fracture. It also presented a wire drawing defect appearing as a crack in the radial-longitudinal plane, which is noticeable on the bottom left image in Figure 10. The apparent crack length in the transversal plane was 800 µm. Due to its orientation – parallel to the tensile direction – the effect of this crack on the strength of the strand was *de facto* limited but its effect on the reduction of area at fracture distinctly appeared.

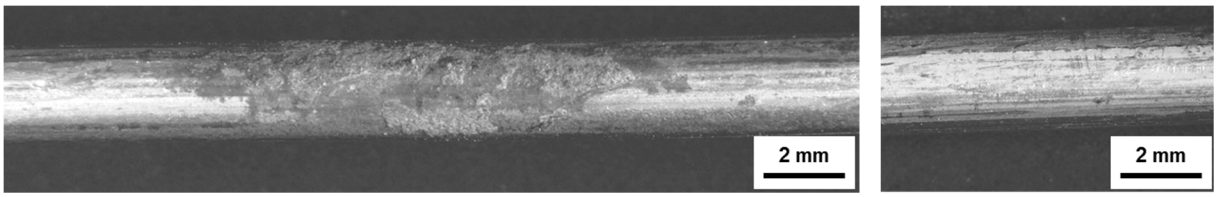

Figure 6: Photographs of galvanized steel strands of the GHW conductor before tensile tests; left: corrosion mark on the external layer strand; right: lower degree of corrosion of the central strand.

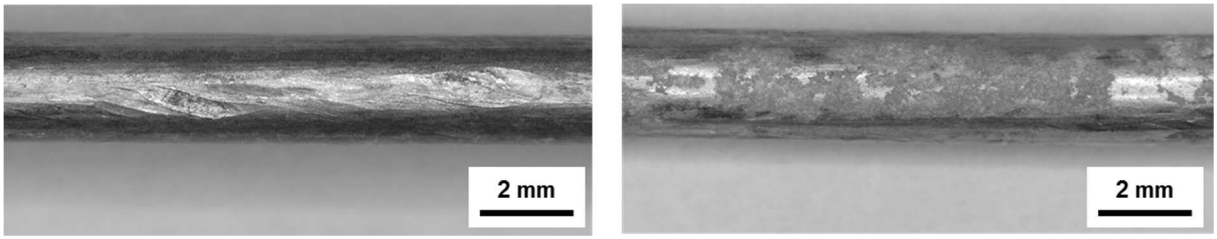

Figure 7: Photographs of a galvanized steel strand from the internal layer of the modern conductor before tensile tests; left: periodic marks due to interaction with the neighboring strands; right: corrosion mark.

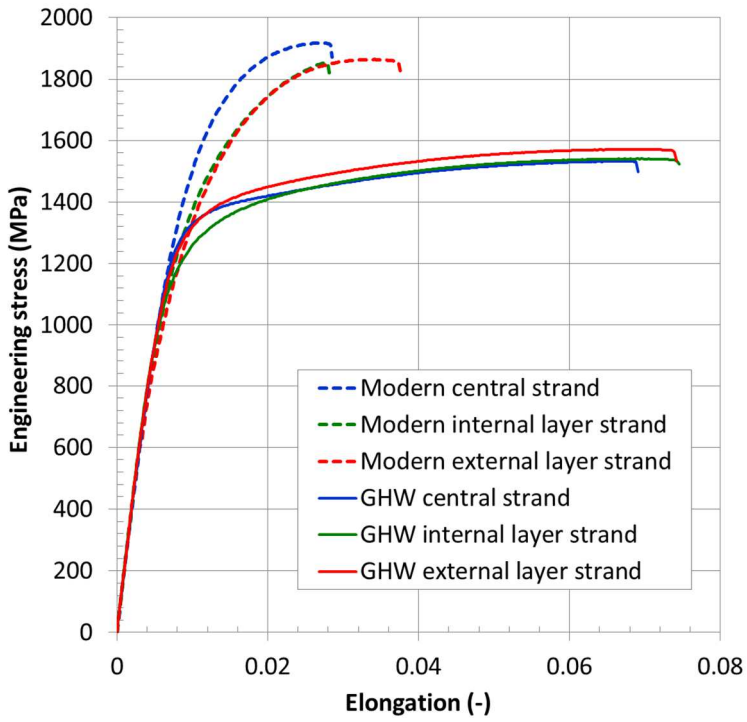

Figure 8: Tensile test curves obtained on the galvanized steel strands extracted from both the GHW and the modern conductors.

Table 2: Mechanical properties of the galvanized steel strands extracted from both the GHW and the modern conductors.

	0.2 % yield stress (MPa)	Ultimate tensile strength (MPa)	Uniform elongation (plastic) (-)	Elongation at fracture (-)	Total uniform elongation (elastic + plastic) (-)	Reduction of area at fracture (-)
GHW central strand	1258	1533	0.061	0.062	0.068	0.28
GHW internal layer strand	1154	1541	0.061	0.067	0.068	0.44
GHW external layer strand	1226	1572	0.061	0.067	0.068	0.44
Modern central strand	1383	1917	0.018	0.020	0.027	0.45
Modern internal layer strand	1213	1853	0.019	0.019	0.028	0.40
Modern external layer strand	1120	1864	0.025	0.029	0.034	0.40

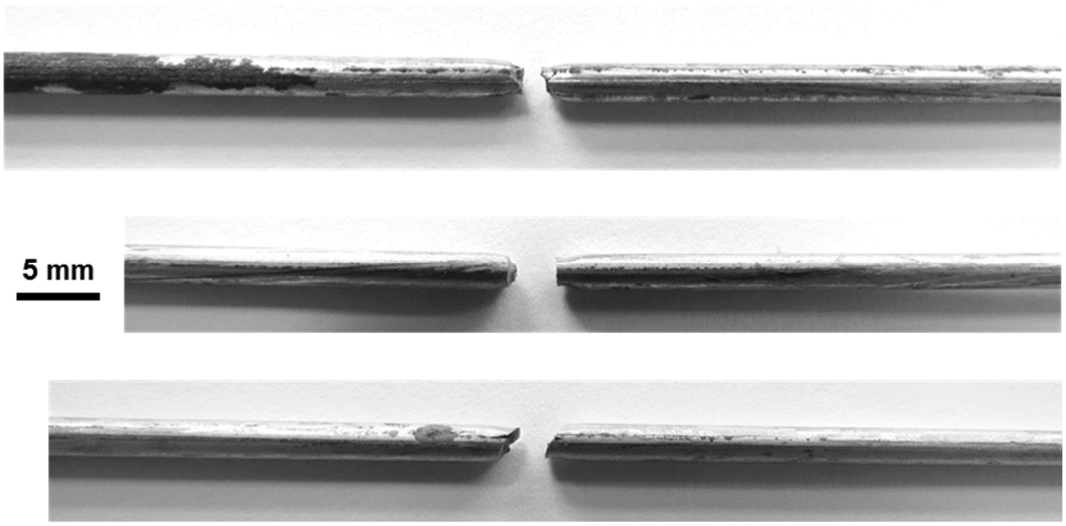

Figure 9: Photographs of the galvanized steel strands of the GHW conductor after tensile tests; top: fracture of the external layer strand initiated away from the main corrosion mark; middle: internal layer strand; bottom: central layer strand.

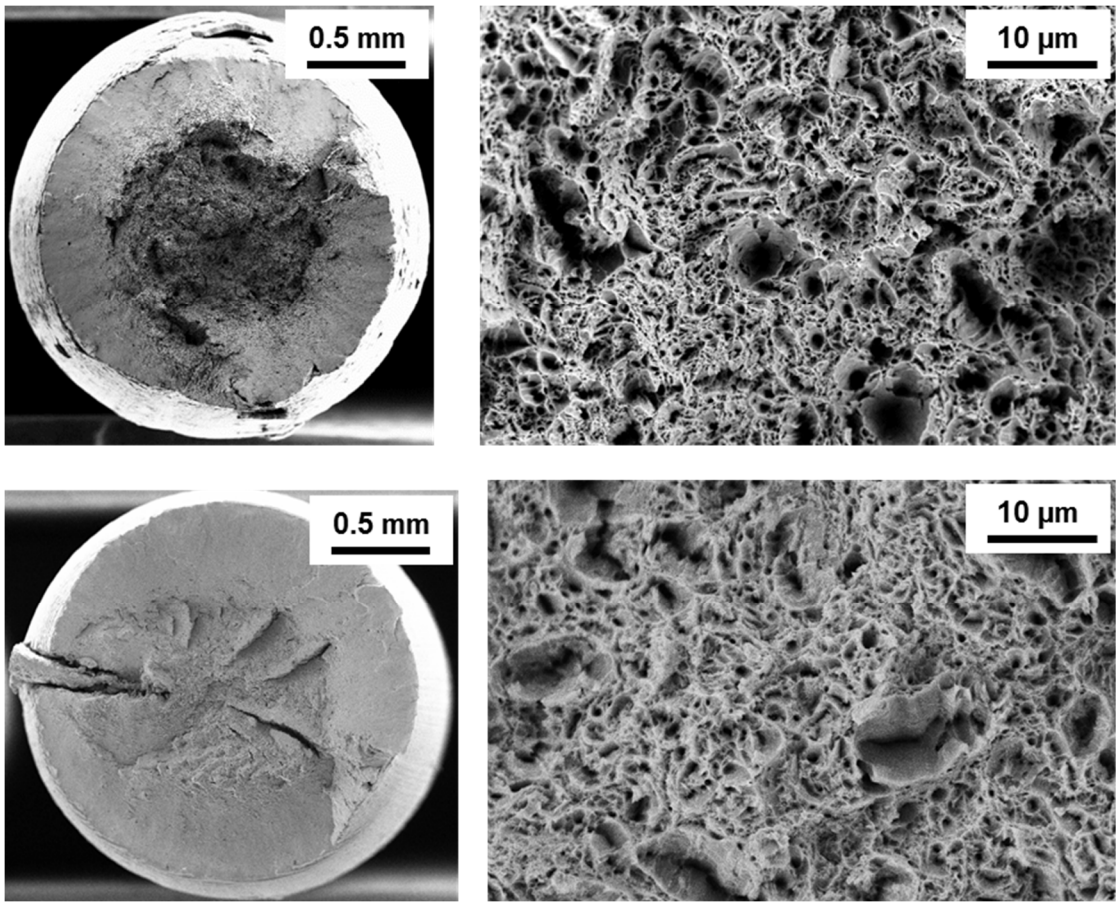

Figure 10: SEM images of the fracture surface of galvanized steel strands extracted from the GHW conductor; top: external layer strand; bottom: central layer strand; left: general views; right: detailed view of the numerous dimples located in the central area.

3.2 Aluminum strands

3.2.1 Microstructure and hardness

The average hardness of the aluminum strands was between 40 and 43 HV for the GHW conductor and between 45 and 50 HV for the modern conductor. In both cases, no significant difference in the hardness value of the different strands was noticed.

The external layer strands of the modern conductor strands had a native smooth passivated surface. Concerning the GHW external strands, the zone exposed to the environment exhibited signs of atmospheric corrosion with the presence of pits. Some of these pits were filled with cracked aluminum oxide containing phosphorus and sulfur (Figure 11). The depth of the pits was inferior to 100 µm. Some areas presented an oxide layer, which had a maximum thickness of 5 µm. It was generally associated with corrosion pits.

For both the GHW and the modern conductors, no sign of corrosion was detected on the inner strands or on the zones that were not exposed to the environment on the external layer. On every aluminum strand, signs of plastic deformation were noticed due to the interaction with the neighboring strands, made of either aluminum or galvanized steel (Figure 12).

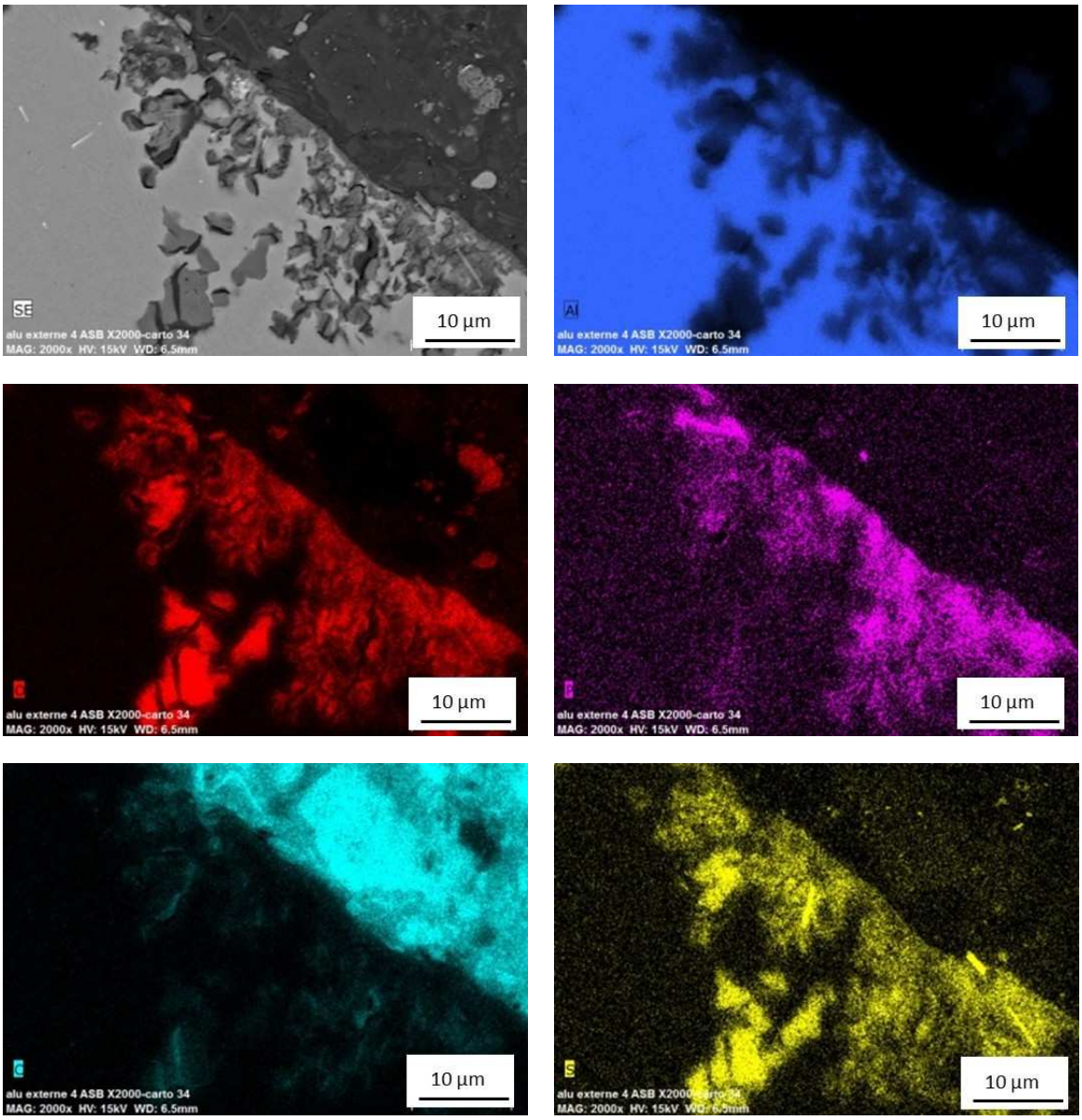

Figure 11: SEM image and EDS analysis of a cross section of an external aluminum strand extracted from the GHW conductor. Aluminum is in blue, oxygen in red, carbon in cyan, sulfur in yellow and phosphorus in pink.

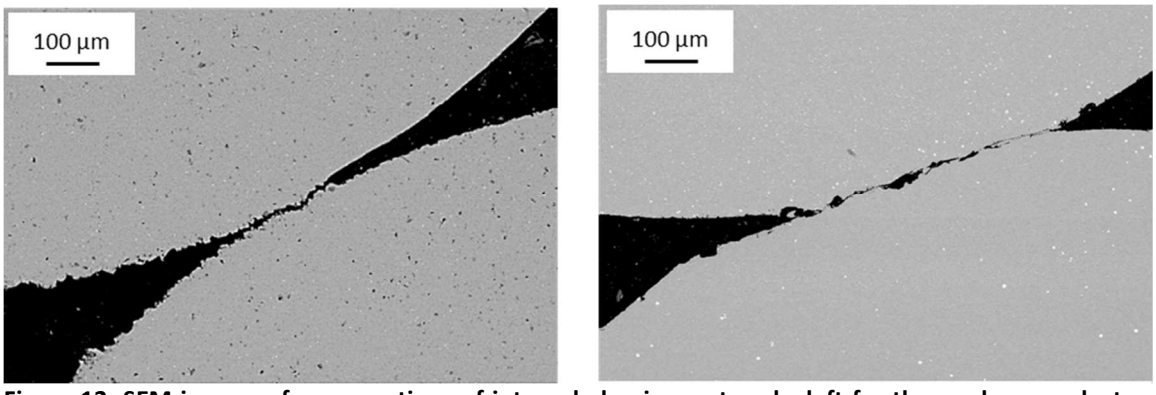

Figure 12: SEM images of cross sections of internal aluminum strands; left for the modern conductor; right for the GHW conductor.

3.2.2 Tensile tests, pre- and post-test characterization

Before the tensile tests, the aluminum strands were visually examined and their diameter was measured: 3.54 ± 0.01 mm and 3.55 ± 0.01 mm, for those extracted from the GHW and from the modern conductor, respectively. Noticeable on every strand were the periodic marks due to the interaction with the neighboring steel or aluminum strand layers (left picture in Figure 13 and in Figure 14). The periodic marks on the modern conductor strands were as pronounced as the ones on the GHW, indicating that they originated from the manufacturing process rather than from a potential degradation during operation. Visual examination also confirmed the presence of numerous atmospheric corrosion pits all along the external part of the external layer strands of the GHW conductor (right picture in Figure 13). The diameter of these pits was approximately 0.1 mm. The inner part of the external layer strands and the inner layer strands were exempt of pits. In places, the external part of the external layer strands also presented some squashing marks (right picture in Figure 14).

Tensile test curves are presented in Figure 15. Mechanical properties resulting from these tests are reported in Table 3. As expected from the hardness values (*cf.* section 3.2.1), the tensile strength of the aluminum strands extracted from the modern conductor was higher than the one of the strands extracted from the GHW conductor. Noticeable was the important reduction in area (> 0.8) and the relatively low total uniform elongation (~0.01) of all the tested aluminum strands. The two lowest obtained total uniform elongation values corresponded to the two external layer strands of the GHW conductor.

Post-test observations by optical means and by SEM indicated that the fracture was in all cases completely ductile with an important reduction in area and numerous dimples on the fracture surfaces (right part of Figure 16). Atmospheric corrosion pits were noticed on the external part of the aluminum external layer strands of the GHW (top left image in Figure 16). Apart from these pits, SEM images of the modern conductor aluminum strands – not reported here – presented features similar to the ones of the GHW conductor. As shown in Figure 17, the fracture of the aluminum external layer K strand of the modern conductor was initiated on the squashing mark observed before fracture (right picture in Figure 14), whereas the fracture of the other studied external layer strand was not related to any mark. Nevertheless, the mechanical properties of these two strands were very close (Figure 15 and Table 3). Consequently, this mark was slight enough not to have impaired the mechanical properties of the strand.

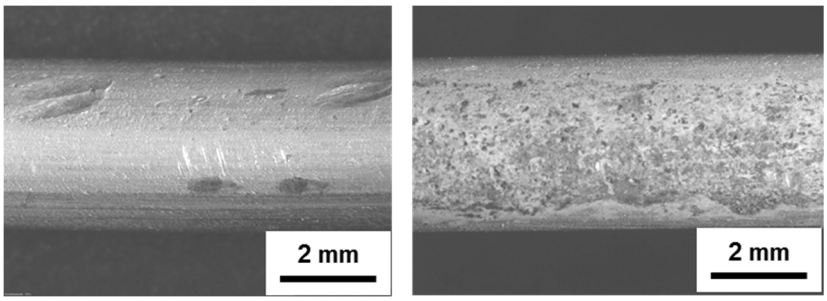

Figure 13: Photographs of aluminum strands of the GHW conductor before tensile tests; left: periodic marks on the internal layer I strand due to interaction with the neighboring steel strands; right: numerous corrosion pits on the external surface of the external layer A strand.

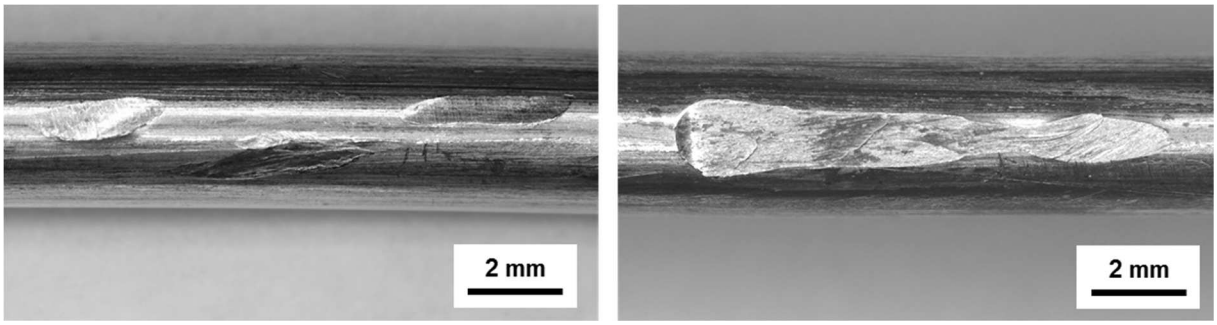

Figure 14: Photographs of aluminum strands of the modern conductor before tensile tests; left: periodic marks on the internal layer H strand due to interaction with the neighboring steel strands; right: mark on the external surface of the external layer K strand.

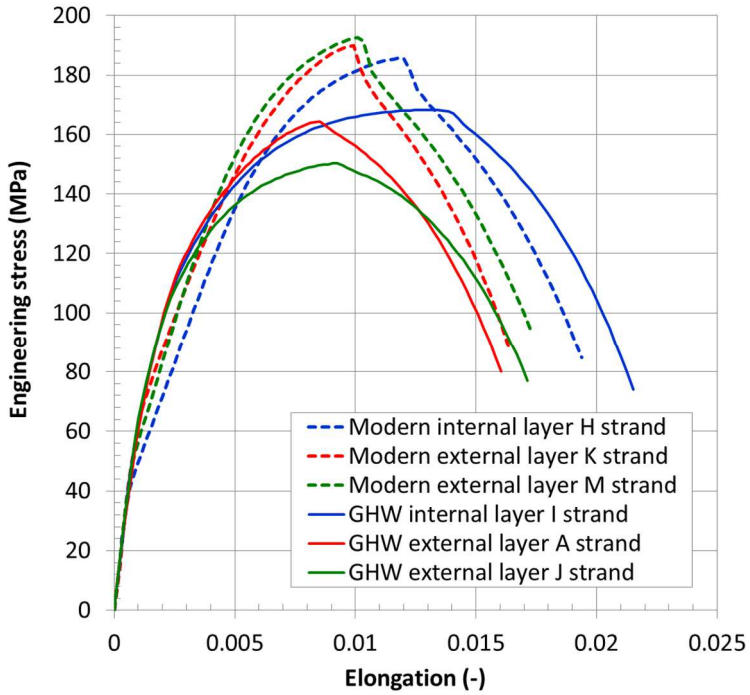

Figure 15: Tensile test curves obtained on the aluminum strands extracted from both the GHW and the modern conductors.

Table 3: Mechanical properties of the aluminum strands extracted from both the GHW and the modern conductors.

	0.2 % yield stress (MPa)	Ultimate tensile strength (MPa)	Uniform elongation (plastic) (-)	Elongation at fracture (-)	Total uniform elongation (elastic + plastic) (-)	Reduction of area at fracture (-)
GHW internal layer I strand	131	168	0.011	0.020	0.013	0.89
GHW external layer A strand	133	164	0.006	0.015	0.009	0.88
GHW external layer J strand	125	150	0.007	0.016	0.009	0.87
Modern internal layer H strand	105	186	0.009	0.018	0.012	0.86
Modern external layer K strand	125	190	0.007	0.015	0.010	0.84
Modern external layer M strand	131	193	0.007	0.016	0.010	0.87

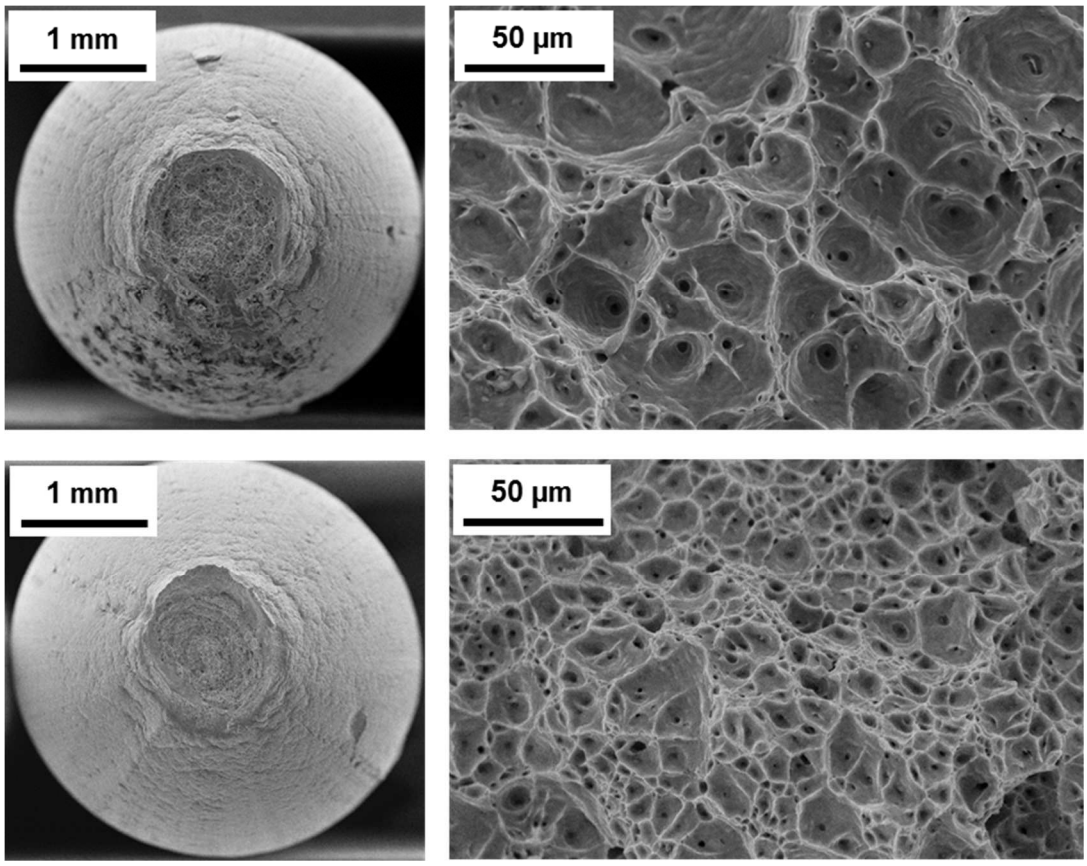

Figure 16: SEM images of the fracture surface of aluminum strands extracted from the GHW conductor; top: external layer J strand; bottom: internal layer I strand; left: general views; right: detailed view of the numerous dimples located in the central area.

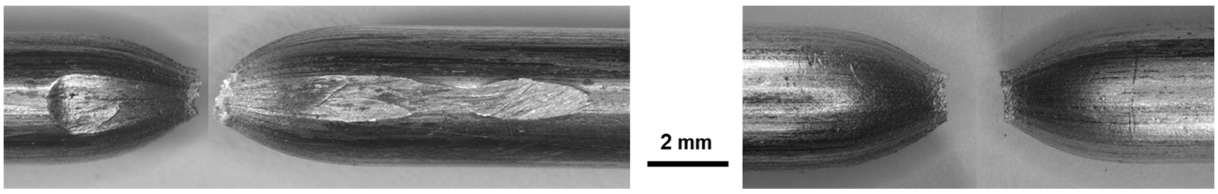

Figure 17: Photographs of the aluminum strands of the modern conductor after tensile tests; left: fracture of the external layer K strand initiated on the mark observed before the test (Figure 14); right: fracture of the external layer M strand.

3.3 Grease

One sample of each conductor was analyzed by FTIR in order to give insight into the grease formulation and its potential ageing. Infrared spectra obtained over the frequency range from 600 to 4000 cm^{-1} are shown in Figure 18. On both spectra, noticeable were the intense absorption near 2900 cm^{-1} resulting from asymmetric and symmetric stretching of CH and the peaks at 1460, 720 and 1376 cm^{-1} corresponding to bending of CH_2 for the first two and CH_3 for the last.

The modern sample spectrum also presented some similarities to the spectrum of pure water [32]: two broad absorption bands, the most prominent one ranging from 3000 to 3700 cm^{-1} corresponding to OH stretching and the smaller one at 1636 cm^{-1} corresponding to OH bending. This analysis therefore indicated that the grease of the modern conductor contained an important amount of water. The spectrum of the GHW sample also presented a peak near 1600 cm^{-1} but presented only two very small peaks around 3400 cm^{-1}, indicating a major difference between the water content of the two samples. Another difference was the presence in the spectrum of the GHW sample of a strong peak around 1700 cm^{-1}, which corresponded to the C=O double bond stretching. This could be a sign of the oxidation of the grease during service [18].

In the fingerprint region, a multitude of mainly C-C stretching and C-H bending modes was present resulting in a very dense structure of overlapping lines. These C-C stretching and C-H bending modes peaks were more intense on the spectrum of the GHW sample than on the spectrum of the modern one, which confirmed that the GHW grease did not contain as many -OH groups as the modern grease.

Chemical analysis of the degreasing baths indicated the predominance of the following five elements: zinc, aluminum, iron, calcium and copper (Table 4). The first three were constitutive of the conductors. Calcium most probably originated from the complex soap used as thickener for the grease [18], copper is also a common additive. Noticeable was also the much lower amount of lead in the grease of the modern conductor than in the grease of the GHW conductor. The characteristics of the grease used in the 50s were indeed different from the more recent ones, with increasing drop points: from 60 °C in 1965 to 110 ° C in 1976 and decreasing lead content to reduce pollution [33].

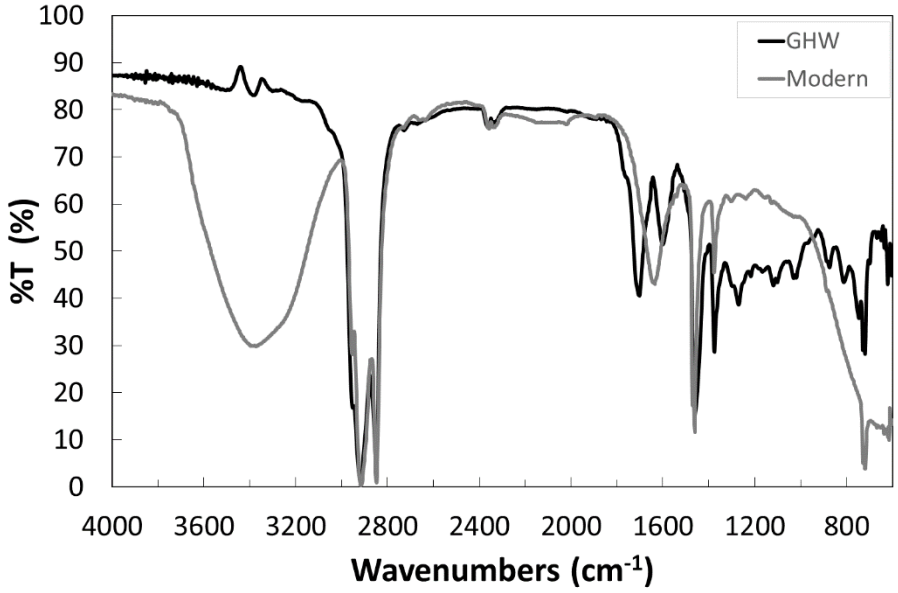

Figure 18: FTIR analysis of the grease of the two conductors.

Table 4: Composition of degreasing baths expressed in mg.kg^{-1}. Measurements of metal contents were made by ICP-MS.

Conductors	Al	Ca	Fe	Zn	B	Cu	Na	Cr	Mg	Si	K	Pb
Modern	2230	1385	1470	4022	261	448	726	97	56	355	42	5
GHW	4452	5014	3529	3549	130	1493	642	176	206	227	182	156

3.4 Summary of the characterization results

The characterizations showed that both studied conductors were in a relatively good general state although some signs of physicochemical degradations were visible. Physicochemical degradations referred to the partial oxidation of the galvanization layer of the steel strands, to the atmospheric corrosion pits of the aluminum external layer and to the oxidation of the grease. As expected due to ageing during more than 60 years of operation, the GHW conductor showed more signs of physicochemical degradation than the modern sample (Table 5). Other features were noticed during the characterization but were not classified as degradations as they seemed to originate from the manufacturing or online installation processes: longitudinal cracks due to wire drawing, periodic marks due to the interaction of the strands with the neighboring layer strands, squashing marks on the aluminum strands of the outermost layer. Also reported in Table 5 are the main mechanical properties of the strand. These results are discussed in section 4.

Table 5: Summary of the characterization results of the GHW and the modern conductors.

		GHW	Modern
Galvanized steel strands	Depth of the oxidation of the galvanization layer (μm)	up to 20	< 5
	Thickness of the residual un-oxidized galvanization layer (μm)	5-20	> 25
	Cross section apparent length of the cracks originated from the wire drawing process (μm)	up to 800	< 15
	Hardness (HV)	420 - 470	490 - 520
	Minimum ultimate tensile strength (MPa)	1533	1853
	Minimum elongation at fracture (-)	0.062	0.019
	Minimum reduction of area at fracture (-)	0.28	0.40
Aluminum strands	Atmospheric corrosion pits on the surface of the external layer	Yes	No
	Width of the marks due to interaction between strands of neighboring layers (mm)	0.5 - 1	0.5 - 1
	Hardness (HV)	40 - 43	45 - 50
	Minimum ultimate tensile strength (MPa)	150	186
	Minimum elongation at fracture (-)	0.015	0.015
	Minimum reduction of area at fracture (-)	0.87	0.84
Grease	Presence of water	No	Yes
	Signs of oxidation (C=O double bound)	Yes	No

4 Discussion

The main purpose of the present study was to characterize an ACSR conductor extracted from a 225 kV overhead transmission line, which had been operated since 1950. The characterizations showed a twofold degradation: (i) degradation of the strands by corrosion, and (ii) degradation of the grease. Each point plays a role in the different phases of the life of the conductors. The discussion is divided into three parts. The analysis of the galvanization layer degradation is discussed in a first part. The mechanical properties that might be affected by these degradations are presented in a second part. The discussion section ends with the estimation of the tensile strength of the studied conductors.

4.1 Degradation of the galvanization layer of the steel strands

The steel strands of both the GHW conductor and the modern one were galvanized. In both cases, the galvanization layer initially consisted of sublayers: intermetallic with iron and zinc on the steel side and pure zinc on the outside, as illustrated in Figure 2 for the modern conductor and in Figure 3(c) for the GHW conductor in places where the steel strand was embedded in the aluminum strand.

The absence of the pure zinc eta phase sublayer on most galvanized steel strands from the GHW conductor showed that the galvanization layer had degraded during operation. The characterization indicated that this degradation was due to a corrosion phenomenon. Indeed, some corrosion products (ZnO) located on the external surface of the galvanization layer were observed (Figure 3(b)) and identified by Raman spectroscopy (Figure 4). They did not appear very adherent to the layer and contained many cracks.

Based on these characterizations, a three-step degradation mechanism of the galvanized steel strands is proposed (Figure 19). At first, the conductor is new and exposed to the environment (Figure 19(a)). Since the grease limits the interaction with the environment, the galvanization layer is only weakly corroded (Figure 19(b)), which results in a thin layer of oxide, as observed on the surface of the modern sample (Figure 2). Then, this corrosion phenomenon progresses until complete oxidation of the eta phase thus forming a zinc oxide layer ZnO (Figure 19(c)). This oxide has a Pilling and Bedworth ratio (PBR) of 1.55 [34], which induces an internal stress and may cause cracking as the thickness increases, making it more brittle and less adherent. Due to this brittleness and to the mechanical loading (macroscopic stress, local stress due to the interaction between the strands and internal stress), the oxidized phase spalls off, leaving the intermetallic sublayer, partially oxidized, with punctual remaining parts of the ZnO layer (Figure 19(d)).

The purpose of the present paragraph is to discuss the corrosion mechanism of the zinc sublayer. To initiate a phenomenon of corrosion an electrolyte is necessary. The first hypothesis considered is an infiltration of water. This hypothesis is commonly mentioned in the literature [13, 22-24, 35]. If infiltration is possible, keep in mind that the modern cable was never in service and was more recent than GHW. Also, the inner aluminum layer on the non-zinc side of GHW was not corroded. If there was infiltration, it should have been corroded. The presence of ZnO on GHW and in a small quantity on the modern cable tends towards that there may have been infiltration but it is not the only explanation for the condition of the cable after 60 years of operation. Second hypothesis to be examined is the presence of grease and its degradation. The conductors were greased on all the layers except the outermost. FTIR analysis of the grease of the modern conductor indicated that it contained a lot of water. On the contrary, the absence of the-OH peak in the GHW grease FTIR spectrum showed that the grease had been oxidized, which was also consistent with the presence of an additional peak around 1700 cm^{-1}. This peak was due to the C=O double bond of the ketones and characteristics of the oxidation of lubricating products [18]. During this oxidation, the carbon

structure was conserved which is in agreement with the FTIR spectra. Moreover, this reaction led to the creation of water.
These two hypotheses are not antagonistic and show that in both cases an electrolyte was created, which can lead to a corrosion phenomenon. Graedel showed that the corrosion of a zinc surface takes place in several stages. The first product formed is zinc hydroxide $Zn(OH)_2$ [36]. This hydroxide tends to dehydrate to form ZnO. On the other hand, from the data of the literature, a galvanic coupling between aluminum and zinc is possible. The gravity of the galvanic corrosion, however, can not be predicted from the potential values of the constituents of the couple, which only reflect the electrochemical aspect of the galvanic corrosion. However, this galvanic coupling could explain why the aluminum strands were not corroded (apart from the atmospheric corrosion of the external side).

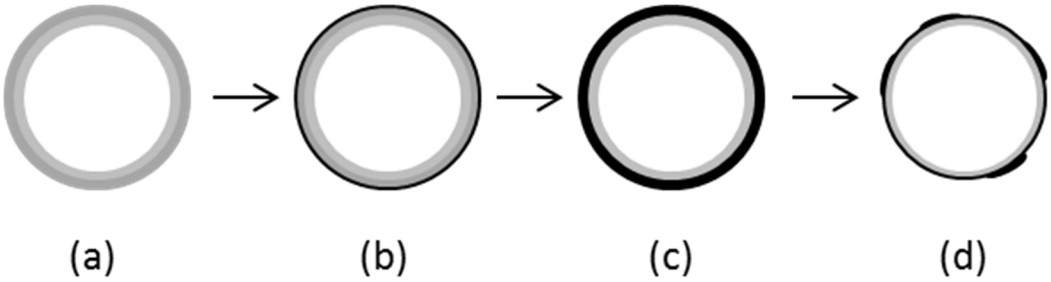

Figure 19: Diagram of the proposed degradation mechanism of the galvanized steel strands. Steel is represented in white at the center of the strand. The different sublayers of the galvanization layer are represented in gray. The zinc oxide is represented in black. (a) a new strand, (b) strand with a superficial corrosion of the eta layer, (c) the corrosion phenomenon progressed until complete oxidation of the eta phase and (d) the oxidized phase spalled off, leaving the intermetallic sublayer, partially oxidized, with punctual remaining parts of the ZnO layer.

4.2 Mechanical properties of the strands

Regarding the tensile strength of aluminum strands, the French standards edited in 1955 [37] required a minimum value of 167 MPa. The ultimate tensile strength of the aluminum strands extracted from the GHW were 168 MPa, 164 MPa and 150 MPa for the internal layer strand and the external layer strands, respectively (Table 3). Regarding the elongation at fracture of aluminum strands, the minimum value required was 0.020, whereas the obtained values were 0.020, 0.015 and 0.016 for the internal layer strand and the external layer strands, respectively (Table 3). Therefore the mechanical properties of the external layer aluminum strands were slightly lower than the requirements of the standards edited in 1955, whereas the mechanical properties of the internal layer aluminum strand were slightly higher. As the main apparent difference between the strands from these two layers was the presence/absence of atmospheric corrosion pits, it might be related to the mechanical properties. Further investigation on more severely corroded samples should help establishing and quantifying this relation. More recent standard [29]required a minimum tensile strength value of 152 MPa and did not specify the minimum elongation at fracture. As the minimum ultimate tensile strength obtained on the aluminum strands extracted from the modern conductor was 186 MPa (Table 3), they fulfilled, as expected, this requirement.

Requirements of the French standards [29, 38-40] regarding the tensile strength and the elongation at fracture of galvanized steel strands are reported in Figure 20 together with the corresponding values obtained on the strands extracted from the GHW and the modern conductors. The minimum required tensile strength increased during the second half of the 20th century whereas the minimum

elongation at fracture decreased. This figure also indicates that, after more than 60 years of operation, the galvanized steel strands from the GHW conductor still fulfilled the requirement edited at the time they were brought into operation. The partial corrosion of the galvanized steel strands described in the previous sections was sufficiently superficial not to have affected their mechanical properties. The fracture of the strands did not initiate on corrosion marks. However, these 60 years old strands did not fulfill the more recent and more demanding requirements for the tensile strength (Figure 20). As expected, the galvanized steel strands extracted from the modern conductor had a higher strength and a lower ductility. They fulfilled all the requirements for the tensile strength and the most recent requirements for elongation at fracture but not the older ones (Figure 20).

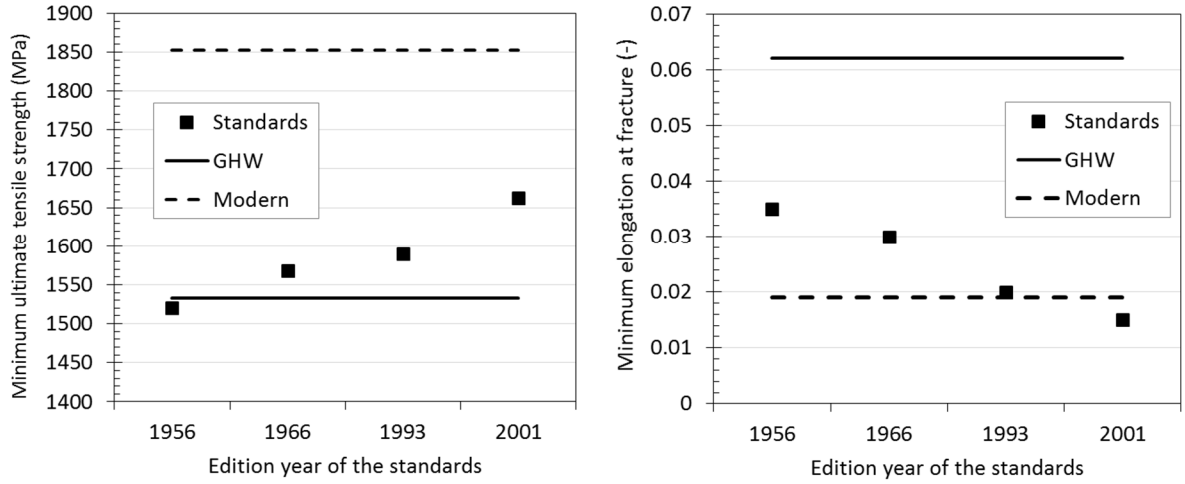

Figure 20: Minimum ultimate tensile strength (left) and minimum elongation at fracture (right) measured on the studied galvanized steel strands from the GHW and the modern conductors in comparison to the requirements of the French standards edited in 1956, 1966, 1993 and 2001 [29, 38-40].

4.3 Estimation of the tensile strength of the studied conductors

Lanteigne and Akhtar proposed and validated a theoretical model allowing to infer the conductor elastoplastic mechanical behavior from the mechanical behavior of its constitutive strands [41, 42]. In the framework of the present study, an extremely simplified version of this modelling was used to illustrate the potential effect of the corrosion of aluminum strands on the tensile strength of ACSRs. Neglecting the lay angle, the stress and strain due to stranding and straightening and the interactions between the strands, the conductors were considered as a juxtaposition of parallel strands. Due to the long length of the conductors, total – elastic plus plastic – elongation at fracture was assimilated to the total uniform elongation. As the total elongation of the aluminum strands was much lower than the one of galvanized steel strands, for both the GHW and the modern conductors, the aluminum strands were predicted to break first. Consequently, the tensile strength of the conductor could be estimated by Eq. 1. In this equation, UTS stands for ultimate tensile strength, A for cross-section area and $\sigma_{steel}(TE_{steel}=TUE_{aluminum})$ for the stress corresponding to a total elongation of the galvanized steel strand that is equal to the total uniform elongation of the aluminum strands.

Using Eq. 1, the nominal cross-section areas of the conductors and the results of the tensile tests done on the strands, the tensile strength of the GHW and the modern conductors were estimated to be 160 kN and 183 kN respectively. The corresponding standard requirements were 155 kN [37] and 173 kN [29], in 1955 and 2001 respectively. Therefore, following this modelling, the GHW conductor

should still, after 60 years of operation, fulfill the tensile strength requirement from the time it was brought into operation but not those from current standards. As expected, based on the same modelling, the estimation of the tensile strength of the modern conductor was higher than the current requirements.

Although very simple, this modelling illustrates the fact that the total uniform elongation of aluminum strands is a key parameter in the determination of the tensile strength of ACSRs. No matter the ultimate tensile strength of the galvanized steel strands, because during a tensile test on such a conductor the aluminum strands break long before the steel could possibly reach such a stress. This fact also explains why the steel strands elongation requirements decreased during the second half of the 20th century in order to increase their minimum yield stress.

As the lowest values of the total uniform elongation were obtained – in the present study – for the external layer aluminum strands, which exhibited some corrosion pits, future investigation will focus on the effect of ageing on the total elongation of aluminum strands.

$$UTS_{conductor} = \sum_{\substack{aluminum \\ strands}} [A_{aluminum} \times UTS_{aluminum}] + \sum_{\substack{steel \\ strands}} [A_{steel} \times \sigma_{steel}(TE_{steel} = TUE_{aluminum})] \quad \textbf{Eq. 1}$$

5 Conclusions

The characterization of an aluminum conductor steel reinforced after 60 years of operation in a mixed rural and urban environment led to the following conclusions:

- Partial oxidation of the galvanization layer of the steel strands led to the formation of ZnO and reduction of its effective thickness by approximately 20 µm;
- Degradation of the grease – especially oxidation – due to ageing is thought to be the cause of the oxidation of the galvanization layer;
- The mechanical properties of the galvanized steel strands were still in agreement with the requirements of the standards edited in 1955;
- Atmospheric corrosion of the external layer of aluminum strands caused the formation of numerous pits with a depth inferior to 100 µm, whereas the internal layer of aluminum strands was not corroded due to the protective role played by the grease;
- The mechanical properties of the external layer aluminum strands were slightly lower than the requirements of the standards edited in 1955, whereas the mechanical properties of the internal layer aluminum strand were slightly higher, indicating a potential deleterious effect of the corrosion pits on the mechanical properties of the aluminum strands;
- The tensile strength of the conductor estimated from the mechanical properties of its constitutive strands was slightly higher than the requirements of the standards edited in 1955 and slightly lower than the more demanding requirements of recent standards.

Future work on this topic will focus on the characterization of conductors that operated in more severe corrosive environments or were submitted to higher mechanical loads.

6 Acknowledgements

Delphine Neff from CEA, CNRS, Université Paris-Saclay, is gratefully acknowledged for carrying out the Raman spectroscopy. Fruitful discussions with Christine Yang and Fikri Hafid from RTE are also acknowledged.

7 References

1. Havard DG, Bellamy G, Buchan PG, Ewing HA, Horrocks DJ, Krishnasamy SG, et al. IEEE Transactions on Power Delivery. **1992**;7(2):588-95.
2. Zhang X, Gockenbach E, Wasserberg V, Borsi H. IEEE Transactions on Power Delivery. **2007**;22(1):515-22.
3. Havard DG, Bissada MK, Fajardo CG, Horrwks DJ, Meale JR, Motlis J, et al. IEEE Transactions on Power Delivery. **1992**;7(2):588-95.
4. Rhaiem E, Bouraoui T, Halouani FE. IOP Conference Series: Materials Science and Engineering. **2012**;28(1):012011.
5. Ferguson JM, Gibbon RR. POWER ENGINEERING JOURNAL. **JUNE 1994**
6. Chen G, Wang X, Wang J, Liu J, Zhang T, Tang W. Engineering Failure Analysis. **2012**;19:13-21.
7. Zhou ZR, Cardou A, Fiset M, Goudreau S. Wear. **1994**;173(1–2):179-88.
8. Azevedo CRF, Cescon T. Engineering Failure Analysis. **2002**;9(6):645-64.
9. Azevedo CRF, Henriques AMD, Filho ARP, Ferreira JLA, Araújo JA. Engineering Failure Analysis. **2009**;16(1):136-51.
10. Fadel AA, Rosa D, Murça LB, Fereira JLA, Araújo JA. International Journal of Fatigue. **2012**;42:24-34.
11. Kalombo RB, Martínez JMG, Ferreira JLA, Silva CRMD, Araújo JA. Procedia Engineering. **2015**;133:223-32.
12. Boniardi M, Cincera S, D'errico F, Tagliabue C. Key Engineering Materials. **2007**;348-349:5-8.
13. Forrest JS, Ward JM. Supply Section. **1954**:271-83.
14. Aggarwal RK, Johns AT, Jayasinghe JaSB, Su W. Electric Power Systems Research. **2000**;53(1):15-22.
15. Linares L, Taborda N, Zambrano L, Perez. Proc 2006 IEEE PES Transmission and distribution Conf Expo Latin America, Venezuela. **2006**.
16. Elshawesh F, Agaili MEL, Elwaer A. British Corrosion Journal. **1997**;Volume 32 (Issue 1):Pages 77-80.
17. Ito I, Chiba H, Onodera M. CIGRE **2012**;B2_213_2012.
18. Peng AYM, Lyon SB, Thompson GE, Johnson JB, Wood GC, Ferguson JM. British Corrosion Journal. **1989**;24(4):257-64.
19. Isozaki M, Adachi K, Hita T, Asano Y. Electrical Engineering in Japan. **2008**;163(1).
20. Moreira PLDF, Lourenco PM, Lourenco CRSH, Sebrao MZ, Sant'anna I, Wavrik JFaG. Internal Corrosion in Conductor Cables of Power Transmission Lines: Characterization of the Atmosphere and Techniques for Faults Detection. 2009. Available from: http://www.iiis.org/CDs2008/CD2009SCI/IMETI2009/PapersPdf/F174NN.pdf.
21. Azevedo CRF, Henriques AMD, Pulino Filho AR, Ferreira JLA, Araújo JA. Engineering Failure Analysis. **2009**;16(1):136-51.
22. Lyon SB, Thompson GE, Johnson JB, Wood GC, Ferguson JM. Corrosion. **1987**;43(12):719-26.
23. Greenfield EW, Everhart EW. Power Apparatus and Systems, Part III Transactions of the American Institute of Electrical Engineers **1957**;Volume:76(Issue: 3):106 - 17.
24. Håkansson E, Predecki P, Kumosa MS. Reliability, IEEE Transactions on. **2015**;64(3).
25. Vera R, Delgado D, Rosales BM. Corrosion Science. **2006**;48(10):2882-900.

26. Kreislova K, Jaglova M, Turek L, Koukolova A. Koroze a ochrana materialu. **2013**;57 ((1)):25-34.
27. Denby B, Sundvor I, Cassiani M, Smet PD, Leeuw FD, Horálek J. Science of The Total Environment. **2010**;408(20):4795-806.
28. NF EN ISO 6892-1, octobre 2009, matériaux métalliques, essai de traction, partie 1 : méthode d'essai à température ambiante., (Octobre 2009).
29. Norme NF EN 50182, Conducteurs pour lignes aériennes, conducteurs à brins circulaires, câblés en couches concentriques (December 2001).
30. Marder AR. Progress in Materials Science. **2000**; 45: 191±271.
31. Bernard MC, Goff AH-L, Massinon D, Phillips N. Corrosion Science. **1993**;35(5–8):1339-49.
32. Kiefer J, Frank K, Zehentbauer F, Schuchmann H. Biosensors. **2016**;6(2):13.
33. Mushak P. Lead and Public Health: Science, Risk and Regulation: Elsevier Science; **2011**.
34. Pilling N, Bedworth RJ. Inst Metals. **1923**;29:529.
35. Esaklul KA. Handbook of Case Histories in Failure Analysis, Volume 1: ASM International; **1992**.
36. Graedel TE. Journal of the Electrochemical Society. **1989**;136:193C-203C.
37. Norme NF C34-120 : Conducteurs nus, conducteurs d'aluminium et d'aluminium avec âme d'acier pour lignes aériennes, (June 1955).
38. Répertoire de câbles aériens (EDF), Service des Transports d'Energie, (January 1956).
39. Norme NF C34-120, Conducteurs nus pour lignes aériennes, conducteurs en aluminium-acier pour lignes aériennes, (November 1966).
40. Norme NF C34-120, Conducteurs nus en aluminium-acier pour lignes aériennes, (April 1993).
41. Akhtar A, Lanteigne J. ASME J Eng Mater. **1998**;120:33-8.
42. Akhtar A, Lanteigne J. Journal of engineering materials and technology. **1998**;120(1):39-47.